PROCEEDINGS OF THE ROYAL SOCIETY A

Proc. R. Soc. A (2012) **468**, 913–931
doi:10.1098/rspa.2011.0422
Published online 23 November 2011

Upper and lower limits on the stability of calving glaciers from the yield strength envelope of ice

By J. N. Bassis[1,2,*] and C. C. Walker[1]

[1]*Department of Atmospheric, Oceanic and Space Sciences, and* [2]*Department of Earth and Environmental Sciences, University of Michigan, Ann Arbor, MI 48109, USA*

Observations indicate that substantial changes in the dynamics of marine-terminating ice sheets and glaciers are tightly coupled to calving-induced changes in the terminus position. However, the calving process itself remains poorly understood and is not well parametrized in current numerical ice sheet models. In this study, we address this uncertainty by deriving plausible upper and lower limits for the maximum stable ice thickness at the calving face of marine-terminating glaciers, using two complementary models. The first model assumes that a combination of tensile and shear failure can render the ice cliff near the terminus unstable and/or enable pre-existing crevasses to intersect. A direct consequence of this model is that thick glaciers must terminate in deep water to stabilize the calving front, yielding a predicted maximum ice cliff height that increases with increasing water depth, consistent with observations culled from glaciers in West Greenland, Antarctica, Svalbard and Alaska. The second model considers an analogous lower limit derived by assuming that the ice is already fractured and fractures are lubricated by pore pressure. In this model, a floating ice tongue can only form when the ice entering the terminus region is relatively intact with few pre-existing, deeply penetrating crevasses.

Keywords: ice sheet; glacier; iceberg; calving; fracture; sea level

1. Introduction

The sporadic detachment of icebergs, ranging in size from less than 1 m to hundreds of kilometres, provides an efficient and rapid mechanism for the transfer of ice from the ice sheet to the surrounding oceans. Moreover, observations of increased discharge of ice into the ocean in the wake of the detachment of one or more icebergs from the calving front of glaciers have increasingly illustrated the strong link between calving and ice dynamics. For example, the Larsen B ice shelf disintegrated into a plume of needle-shaped icebergs over a period of just six weeks in 2002 (Skvarca *et al.* 2002; Scambos *et al.* 2003), triggering a sustained increase in the discharge of tributary glaciers that continues to this day (Rignot *et al.* 2004; Scambos *et al.* 2004). Likewise, in Greenland, the floating ice tongue in

*Author for correspondence (jbassis@umich.edu).

Received 13 July 2011
Accepted 25 October 2011

front of Jakobshavn Isbræ, one of Greenland's largest outlet glaciers, disintegrated between 1998 and 2002, resulting in a twofold increase in the discharge of ice into the ocean and retreat of the now grounded terminus (Joughin *et al.* 2004, 2008; Luckman & Murray 2005).

Much of the difficulty in understanding and including iceberg calving into numerical ice sheet models stems directly from the diverse range of calving styles observed across environments and glaciological regimes. For instance, a clear distinction exists between the calving behaviours of glaciers where the termini freely float (called ice shelves or ice tongues) and those where the terminus remains grounded (generically referred to as tidewater glaciers here). Calving from ice tongues and ice shelves is characterized by long quiescent periods with few calving events punctuated by the sudden detachment of one or more tabular bergs with a characteristic size of many times the ice thickness (Lazzara *et al.* 1999). Detachment of these large tabular bergs from ice tongues/shelves is preceded by the formation of rifts (fractures that penetrate the entire ice thickness), which can initiate far upstream of the calving front and propagate for decades prior to the eventual detachment of an iceberg (Bassis *et al.* 2005, 2007; Joughin & MacAyeal 2005).

In contrast, glaciers where the ice remains grounded at the terminus tend to calve much smaller and more frequent icebergs, with a characteristic size comparable to or smaller than the ice thickness. Large-scale rifts are rarely observed in tidewater glaciers, but when they do form they initiate only within a few ice thicknesses of the calving front of glaciers that are very close to buoyancy and icebergs detach from the detachment boundary within a few weeks of formation (Walter *et al.* 2010). Tidewater glaciers often calve most vigorously when the ice thickness near the terminus of glaciers approaches buoyancy. This has given rise to a semi-empirical height-above-buoyancy 'calving law' in which the ice thickness at the terminus is assumed to require a minimum or critical height-above-buoyancy or they will disintegrate (Meier & Post 1987; Van der Veen 1996, 2002; Nick *et al.* 2009, 2010). Despite significant efforts (Benn *et al.* 2007), no physical explanation for this type of behaviour has been found. Moreover, height-above-buoyancy calving laws do not permit the formation of floating ice tongues. This is problematic because the distinction between calving regimes is fluid; Columbia Glacier, a temperate calving glacier in Alaska, recently developed a small temporary floating ice tongue coincident with a change in calving regime to a more rift-like calving process consisting of larger, more sporadic quasi-tabular bergs (Walter *et al.* 2010).

As pointed out by Bassis (2011), fluctuations in terminus position due to the sporadic and discrete nature of calving is incompatible with a purely deterministic calving law that expresses the calving flux solely as a function of internal near-terminus variables. This renders specific predictions about individual glaciers problematic, leading to potentially large errors in sea-level rise projections. The aim of this paper is to place plausible bounds on when (or if) glaciers will retreat and to gain qualitative insight into the calving process. We do so by estimating the maximum ice thickness that can be stably supported at the terminus of glaciers (floating or grounded) and use this upper limit to deduce differences between calving from glaciers with floating versus grounded termini. We also present a lower limit by considering an analogous model in which the ice is already pervasively fractured and can be treated as a quasi-granular material.

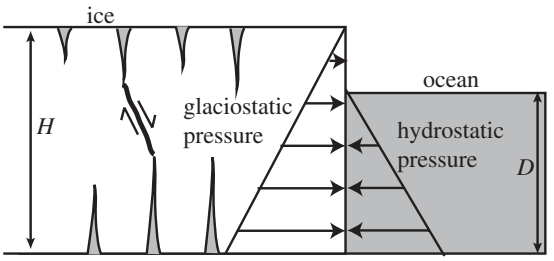

Figure 1. The force balance near a glacier cliff. The conceptual model considered assumes that glacier ice is primarily intact, with isolated surface and basal crevasses that penetrate a portion of the ice thickness. Failure occurs when shear faults connect closely spaced surface and bottom crevasses. Water depth D is measured relative to the bottom of the glacier.

2. Model description

(*a*) *Stress near the terminus of a glacier*

We begin by estimating the state of stress supported by the ice in the near-terminus region. This is accomplished by considering a force balance in the vicinity of a vertical ice cliff of height H, terminating in water of depth D, as illustrated in figure 1. Provided the width of the glacier is large so that horizontal deviatoric and shear stresses associated with the fjord/embayment walls can be neglected, over length scales that are large compared with the ice thickness, the horizontal σ_{xx} and vertical σ_{zz} stresses are approximately (MacAyeal 1989)

$$\sigma_{zz} = -\rho_i g z - S_{xx} \tag{2.1}$$

and

$$\sigma_{xx} = -\rho_i g z + S_{xx}. \tag{2.2}$$

In the above equations, S_{xx} is the horizontal deviatoric stress, ρ_i is the density of ice ($920\,\mathrm{kg\,m^{-3}}$) and g is the acceleration due to gravity ($9.8\,\mathrm{m\,s^{-2}}$), and we have made use of the incompressibility condition to eliminate the vertical deviatoric stress S_{zz} using the relationship $S_{zz} = -S_{xx}$. The net deviatoric stress S_{xx} results from the imbalance between the weight of the ice and the water–air in front of the ice and is determined by balancing the depth-averaged horizontal stress with the depth-averaged pressure due to water at the interface adjacent to the ice cliff (Van der Veen 1996),

$$\int_0^H (-\rho_i g z + S_{xx})\,\mathrm{d}z = \int_0^D -\rho_w g z\,\mathrm{d}z, \tag{2.3}$$

where ρ_w ($1020\,\mathrm{kg\,m^{-3}}$) is the density of water in front of the terminus, assumed to be sea water. Upon integrating, we can solve for the depth-averaged deviatoric stress necessary to satisfy the force balance

$$S_{xx} = \frac{1}{2}\rho_i g H \left[1 - \left(\frac{\rho_w}{\rho_i}\right)\left(\frac{D}{H}\right)^2\right]. \tag{2.4}$$

Equations (2.1)–(2.4) are approximations that hold only in a depth-integrated sense; bending stresses within the ice, lateral shear and back-pressure from any mélange in front of the glacier are neglected in this treatment (Reeh 1968; Hanson & Hooke 2003; Bassis 2010). Nonetheless, the above equations are independent of rheology, requiring only knowledge of ice thickness and water depth. This eliminates the need for a more complicated, fully three-dimensional model that explicitly requires the three-dimensional geometry, temperature field and sliding law for each glacier (Hanson & Hooke 2003). This shall prove to be pivotal in comparing predictions from theory with observational records where little beyond near-terminus ice thickness and water depth are known and even these are often uncertain.

(*b*) *Failure and fracture of ice*

(i) *Tensile failure*

Previous attempts to model the failure of glacier ice have focused on tensile fractures (crevasses), assuming that an iceberg will detach when either a surface crevasse or a bottom crevasse penetrates the entire ice thickness or some critical fraction thereof (Weertman 1980; Rist *et al.* 2002; Benn *et al.* 2007; Nick *et al.* 2010). The depth to which crevasses penetrate can be estimated using the Nye zero-stress model in which surface (d_s) and bottom (d_b) crevasses penetrate to the depth where the net horizontal stress vanishes (Nye 1957; Jezek 1984; Nick *et al.* 2010),

$$d_\mathrm{s} = \frac{S_{xx}}{\rho_i g} \tag{2.5}$$

and

$$d_\mathrm{b} = \frac{\rho_i}{\rho_w - \rho_i}\left(\frac{S_{xx}}{\rho_{ig}} - H_\mathrm{ab}\right), \tag{2.6}$$

where H_ab is the height-above-buoyancy, defined by the relationship

$$H_\mathrm{ab} = H - \frac{\rho_w}{\rho_i} D. \tag{2.7}$$

Figure 2 shows the ratio of surface and bottom crevasse penetration depth as a function of the non-dimensional ratio of water depth to ice thickness with S_{xx} from equation (2.4). Bottom crevasses form in water that is greater than or equal to 70 per cent of the thickness of the ice. Even when it is assumed that surface and bottom crevasses intersect, the combined depth of both surface and bottom crevasses does not penetrate more than approximately half the ice thickness. Substantially deeper crevasse penetration depths are possible through a host of mechanisms (e.g. surface meltwater, higher order bending stresses and/or fracture mechanics can be invoked). Here, the Nye zero-stress model is taken as a heuristic, but plausible estimate of the depth to which crevasses can penetrate. Rather than invoking additional means by which crevasses may

penetrate deeper into the ice (e.g. presence of meltwater), we instead consider the possibility that iceberg calving may result from a combination of tensile and shear fracture.

(ii) *Shear failure*

Although sufficient, the requirement that crevasses penetrate through the entire ice thickness is not necessary; if pre-existing crevasses are present, shear failure along faults may cause slabs of intact ice to detach, or enable surface crevasses to connect to the bed and/or bottom crevasse (figure 1). This viewpoint is supported by observations that show that, in many geological materials, failure occurs through shear failure along faults or slip lines when the shear stress $\Delta\tau$ exceeds the yield stress τ_c (Hughes & Nakagawa 1989; Turcotte & Schubert 2002).

For an ice cliff to be stable, the depth-averaged shear stress must be less than the depth-averaged yield stress. Approximating the σ_{xx} and σ_{zz} as the principal stresses and defining the depth-averaged shear strength of ice τ_c,

$$\bar{\tau}_c = \frac{1}{H}\int_0^H \tau_c \,\mathrm{d}z. \tag{2.8}$$

This requirement can be expressed with the inequality

$$\Delta\tau = \tfrac{1}{2}(\sigma_{xx} - \sigma_{zz}) = S_{xx} \leq \bar{\tau}_c, \tag{2.9}$$

where S_{xx} is given by equation (2.4). In contrast to pure tensile failure, which occurs only in regions of the ice where the total horizontal stress σ_{xx} is positive, the shear stress $\Delta\tau$ is approximately constant throughout the glacier thickness and may trigger whole ice thickness failure of the glacier. Before considering detailed models of the yield strength of ice τ_c, we show how the knowledge of the depth-averaged yield strength allows us to place bounds on the maximum height of a calving cliff.

(*c*) *An upper bound on the ice thickness near the terminus*

An upper bound on the ice thickness at the terminus can be deduced by finding the maximum ice thickness when the integrated stress $\Delta\tau$ exceeds the depth integrated strength of the ice. The most conservative bound assumes that the ice is entirely intact with no crevasses. Using equations (2.4) and (2.9), the maximum stable ice thickness possible at the terminus is given by

$$H_{\max} = \frac{\bar{\tau}_c}{\rho_i g} + \sqrt{\left(\frac{\bar{\tau}_c}{\rho_i g}\right)^2 + \frac{\rho_w}{\rho_i} D^2}. \tag{2.10}$$

For a depth-averaged yield stress of 1 MPa, this predicts a maximum dry calving front height of approximately 220 m. Failure of the cliff is predicted to occur even in the unlikely event that no crevasses are present once the ice cliff exceeds this critical threshold.

In the more likely event that ice near the terminus is crevassed, the fractured portion will be unable to support any stress and the intact portion of the ice must support the entire depth-integrated stress. If the fraction of ice thickness

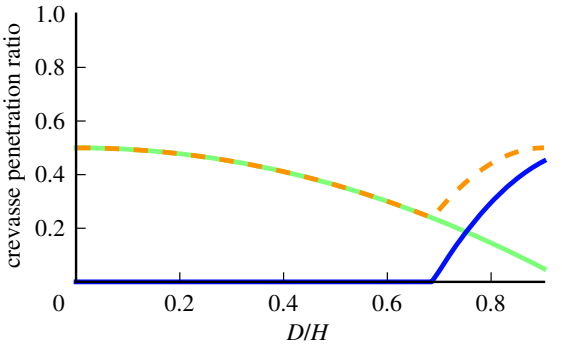

Figure 2. Fraction of the ice penetrated by crevasses as a function of the ratio of water depth to ice thickness at the calving front. The solid green line shows the fraction of the ice thickness penetrated by surface crevasses; the solid blue line shows the fraction of ice thickness penetrated by basal crevasses; the dashed orange line shows the fraction of ice thickness penetrated for the combination of basal and surface crevasses.

penetrated by crevasses is denoted by r and the depth-averaged yield strength is given by

$$\bar{\tau}_c = \frac{1}{H}\int_{d_b}^{d_s} \tau_c \, \mathrm{d}z = r\bar{\tau}_c, \tag{2.11}$$

the maximum stable ice thickness possible at the terminus becomes

$$H_{\max} = \frac{(1-r)\bar{\tau}_c}{\rho_i g} + \sqrt{\left(\frac{(1-r)\bar{\tau}_c}{\rho_i g}\right)^2 + \frac{\rho_w}{\rho_i} D^2}. \tag{2.12}$$

This shows that the apparent strength of crevassed ice is decreased in proportion to the fraction of ice that is fractured; the presence of deep crevasses makes it more likely that the ice will fail even when crevasses do not penetrate the entire ice thickness. This enhancement is purely geometric and neglects additional elastic stress concentrations near the tips of sharp cracks that may be present in the ice. Given that crevasse penetration depths are rarely known and must be estimated, the upper bound implied by equation (2.12) necessarily has a heuristic element. If crevasse depths are calculated using the Nye theory, the maximum dry calving front height possible decreases to approximately 110 m, a value in closer agreement with observed calving front thicknesses that rarely exceed 100 m (Hughes & Nakagawa 1989).

The consequences of the effect of crevasses on the upper bound are illustrated in figure 3, which shows the maximum stable ice thickness as a function of water depth for varying degrees of the fracture penetration parameter r. For each crevasse penetration ratio r, a stable terminus requires an ice thickness–water depth combination that lies to the left of the relevant contour lines. The maximum thickness a dry, grounded ice cliff can support decreases steadily as r increases, with a completely fractured terminus ($r = 1$) encompassing the tensile

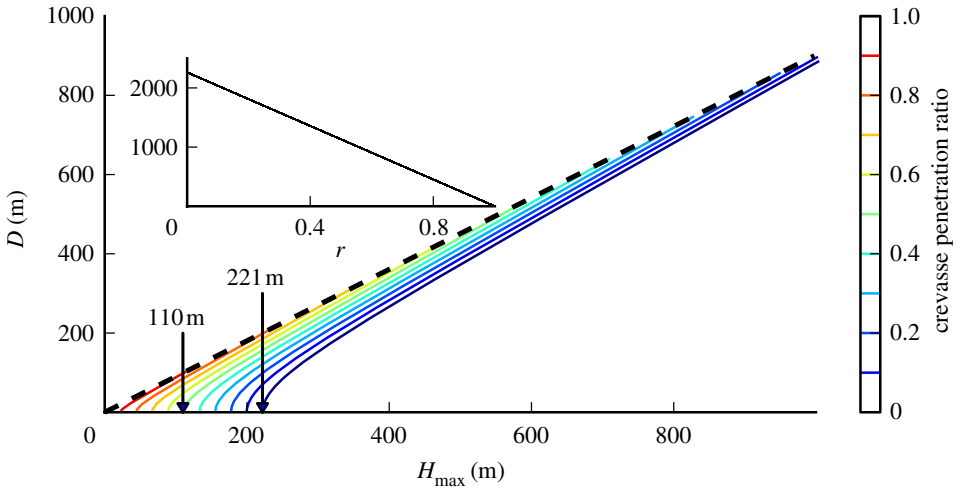

Figure 3. Contours showing maximum stable ice thickness as a function of water depth for different crevasse penetration depths for a constant yield strength of 1 MPa. The contours represent different crevasse penetration ratios r, ranging from 0 (no crevasses) to 1 (completely fractured). The arrows indicate the maximum dry calving cliff thickness when crevasse depths are computed according to the Nye theory (110 m) and when the ice is assumed to be intact with no pre-existing crevasses (221 m). The dashed black line shows the thickness at buoyancy for a given ice thickness. Inset: the maximum floating termini thickness for different fractions of intact ice.

fracture limit considered by other researchers as a special case. An increase in ice thickness decreases the stability of the glacier front, similar to some observations (Brown *et al.* 1982). However, an increase in water depth results in an increase in the stability of the glacier front, contradicting the orthodoxy that increased water depth promotes calving (Brown *et al.* 1982; Meier & Post 1987). A consequence of this is that glaciers that terminate in deep water are able to support larger cliff heights than glaciers that terminate in shallower water. However, once the ice thickness or penetration ratio increases above a threshold, a buoyant ice tongue is no longer stable. Because we assume that, once the water is deep enough to trigger flotation, the ice will float, it is possible to prescribe a critical ice thickness (for each crevasse penetration ratio r) above which a floating ice tongue can no longer be supported (see inset of figure 3). This shows that, in this model, a floating terminus is only possible for glaciers if the ice is not deeply crevassed near the terminus.

More generally, the yield strength may also vary as a function of depth. We suppose that the complete absence of crevasses represents the most aggressive upper limit and assume that the Nye theory provides a working hypothesis that enables us to calculate a first-order estimate of crevasse depths (biased towards the low end compared with linear elastic fracture mechanics). Irrespective of the theory used to calculate crevasse penetration depths, the depth dependence on ice thickness provides a nonlinear inequality, which can be solved numerically (for a given water depth) to obtain an upper bound on the near-terminus ice thickness. Tracing out the upper bound of ice thickness as a function of water

depth provides a stability envelope, and we do this using Brent's bracketed root-finding algorithm (Press *et al.* 1992). Doing so requires a more precise specification of the yield strength for ice, which we consider next.

(*d*) *Yield strength of ice*

Laboratory measurements indicate that shear failure of ice can be described using Coulomb's law (Beeman *et al.* 1988; Schulson 2001), which can be most conveniently expressed in the following form:

$$\tau_c = C_0 + \alpha\rho g(H - z). \tag{2.13}$$

Here, C_0 and α are related to the cohesive strength and coefficient of friction with failure (assumed to occur along optimally oriented planes (e.g. Watts 2001)). As pointed out by Weiss & Schulson (2009), Coulomb failure is often used as a model of both terminal failure of intact materials through shear faulting and the initiation of sliding on pre-existing faults. We shall eventually make use of this distinction, but for now we only require that the parameters C_0 and α are specified, remaining otherwise neutral as to whether the ice is quasi-intact or perforated with pre-existing zones of weakness (faults). More exotic failure relationships beyond Coulomb failure could also be investigated. Particularly relevant for this study, in the absence of friction ($\alpha = 0$), equation (2.13) provides a plastic yield strength (in the Tresca sense) that must be overcome to initiate faulting, similar to the theory originally proposed by Nye *et al.* (1952).

The shear strength of ice appears to depend on a host of factors, including the grain size, size distribution of pre-existing flaws, strain rate, etc. (Schulson & Duval 2009). For a purely granular material without cohesion ($C_0 = 0$), a dry calving cliff with non-zero ice thickness is not possible, unless the coefficient of friction exceeds unity (at that point a dry calving cliff of any height is stable). This contradicts the prevalence of ice cliffs observed in most glaciological settings. For this reason, we consider only yield strengths with cohesion. As a working hypothesis, we adopt three strength models with constant cohesion that represent relatively conservative estimates of the strength of ice. The first strength model (S1) is based on fitting Coulomb's law to frictional sliding experiments on very cold (less than 173 K) saw-cut ice cores (Beeman *et al.* 1988). The failure envelope determined by Beeman *et al.* (1988) indicates a coefficient of friction $\alpha = 0.65$ and a cohesive strength of approximately 1 MPa, a value that is (perhaps coincidentally) comparable to the flexural yield strength for glacier and iceberg ice (Gagno & Gi 1995). Subsequent experiments on warmer ice (-40°C to -10°C) found lower values of friction that were sliding-speed-dependent, but ranged from 0.2 to 0.6 (Kennedy *et al.* 2000). To account for these experiments, we also consider a strength model (S2) that uses the same 1 MPa yield strength as S1, but instead uses a coefficient of friction of 0.4. The last and weakest model we consider assumes either negligible friction or pure plastic yielding ($\alpha = 0$) and a cohesive strength of 1 MPa. Observations of surface crevasses indicate that the cohesive strength of glacier ice might be much smaller (less than 0.5 MPa; Vaughan 1993) so that even our weakest strength model (S3) is conservative in its estimate of the strength of ice.

3. Comparison of theoretical strength envelopes with observations

(*a*) *Data*

To test the validity of the model and the various yield strength envelopes proposed, we assembled measurements of ice thickness and water depth for West Greenland, Alaska and Svalbard from the existing literature. For Alaska, we used the width-averaged water depth and ice thickness reported by Brown *et al.* (1982) for 12 Alaskan glaciers (including Columbia Glacier, Alaska, prior to retreat). Data for Svalbard and West Greenland were obtained from Pelto & Warren (1991) with conversions between per cent buoyant and ice thickness performed using an assumed mean ice density $\rho_i = 920\,\mathrm{kg\,m^{-3}}$. This dataset includes Jakobshavn Isbræ when it still maintained a floating ice tongue. We also included the typical values of ice thickness and water depth reported by Dowdeswell & Drewry (1989) that were based on radio echo sounding flights over Svalbard (115 and 90 m, respectively).

We assembled a more detailed time series of measurements of thickness and water depth for the Columbia Glacier, Alaska, and Helheim Glacier, Greenland. Measurements of water depth and ice thickness for the terminus of the Columbia Glacier were based on bathymetry and photogrammetric images collected by the United States Geological Survey since 1974 and extending up to the year 2000 (Krimmel 2001). Ice thickness and water depths near the terminus were obtained using a weighted nearest-neighbour algorithm with a radius of 500 m (giving all points within 500 m of the point an equal weight, and a weight of zero to all those points outside the radius) to interpolate the velocity, surface elevation and water depth to the terminus. Ice thickness and water depths at the terminus of Helheim Glacier, Greenland, were obtained from three different points during its retreat (5/2001, 8/2003 and 8/2005), using the observations reported by Howat *et al.* (2005).

We used all data as supplied, with the exception of Kongsbreen Glacier, where the reported ice thickness, inferred using the values from Pelto & Warren (1991), exceeded ice thicknesses reported elsewhere (Dowdeswell & Drewry 1989; Lefauconnier *et al.* 1994) and resulted in an ice cliff towering more than 200 m above the water line. Owing to this discrepancy and the fact that we could not track down the original data, we removed these data points from the analysis.

(*b*) *Model data comparison*

Figure 4 compares the stability envelopes computed for the three strength models with the observed combination of ice thickness and water depth. The shaded region in each panel shows regions where a stable terminus is possible, assuming no crevasses (surface or bottom) and that the terminus begins to float if the water is deep enough to permit a buoyant terminus. For each strength model, these limits are assumed to represent the range of permissible ice thicknesses that may be supported at the terminus. The dashed black line in each panel represents the upper bound, which was computed assuming that surface and bottom crevasses penetrate to the depth determined by the Nye zero-stress model. Most of the observations cluster in the lower portions of the graphs, with ice thicknesses and water depths being less than about 400 m. There are several

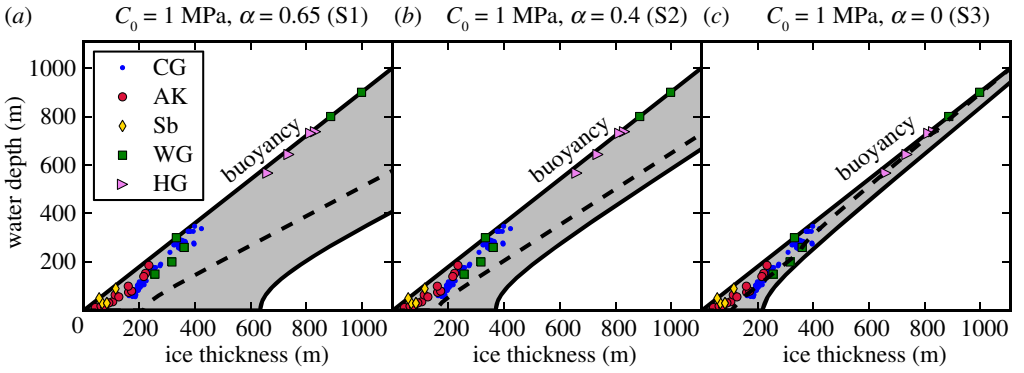

Figure 4. Comparison of observations with predicted critical water depth as a function of ice thickness for three strength models. The shaded region in each figure shows the bounds on allowed ice thickness and water depth combinations assuming no crevasses (bottom or surface). The intersection of the upper bound with the buoyancy line provides the maximum terminus thickness that can be stable. The dashed black line shows the upper limit when bottom and surface crevasses are included. All calculations were performed assuming a density of ice $\rho_i = 920\,\mathrm{kg\,m^{-3}}$ and density of water $\rho_w = 1020\,\mathrm{kg\,m^{-3}}$. CG, Columbia Glacier, Alaska; AK, Alaska; Sb, Svalbard; WG, West Greenland; HG, Helheim Glacier, Greenland.

exceptions owing to the West Greenland tidewater glaciers, whose ice thicknesses near the terminus approach 1000 m. All of these very thick glaciers are close to buoyancy.

From figure 4*a*, it is evident that S1, with no crevasses, provides limits that encompass all of the observations from all of the different regions. The bound, however, appears to be overly conservative in comparison with observed ice thicknesses for all glaciers. The discrepancy is ameliorated somewhat if surface and bottom crevasses are allowed; the lower limit still bounds all of the observations from below, but passes closer to the observations, especially for those glaciers with comparatively thin glacier termini. S2 provides a bound that is closer to the observations and otherwise behaves in a way that is qualitatively similar to S1. S3 provides the tightest fit to all of the data while still managing to bound all of the data from below. Intriguingly, S3 clearly captures the trend in the observations towards glacier termini that are increasingly close to buoyancy for large thicknesses at the terminus. When crevasses are included, the lower limit of S3 no longer bounds all of the observations and instead actually passes close to the centre of the data points. The maximum thickness possible for S3 ranges from about 1100 m without crevasses to a little over 900 m with crevasses. This not only provides a convincing relationship between ice thickness and the maximum ice thickness permissible, it also provides an (approximate) upper bound on the thickness of grounded and floating termini. To our knowledge, glaciers that terminate in cliffs exceeding approximately 1 km in height have not been observed, hinting that this prediction may be robust.

The trend evident in the observations towards decreasing maximum height-above-buoyancy with increasing ice thickness is examined more closely in figure 5, this time specifically for S3. The predicted maximum height-above-buoyancy for S3 matches the observed trend towards the decreasing fraction of ice thickness

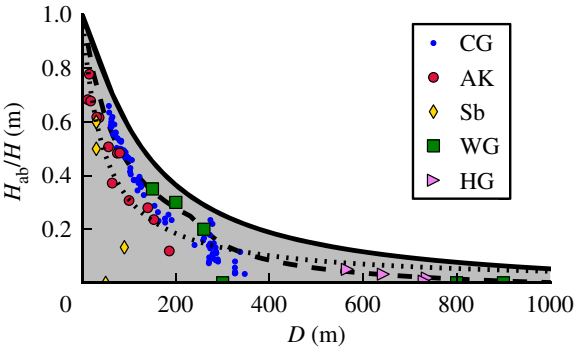

Figure 5. Comparison of observed height-above-buoyancy and water depth against predicted bounds. The shaded region shows allowed values for the height-above-buoyancy determined using S3 ($C_0 = 1\,\mathrm{MPa}, \alpha = 0$) with no crevasses. The dashed black line shows the maximum height-above-buoyancy permitted when surface and bottom crevasses are included. The dotted line shows a constant height-above-buoyancy of 50 m. Density of ice $\rho_i = 920\,\mathrm{kg\,m^{-3}}$ and density of water $\rho_w = 1020\,\mathrm{kg\,m^{-3}}$. CG, Columbia Glacier, Alaska; AK, Alaska; Sb, Svalbard; WG, West Greenland; HG, Helheim Glacier, Greenland.

above buoyancy remarkably well, a fact that is even more surprising because the parameters are empirically derived and values for yield strength have not been tuned to better match observations. All of the observations fall within the shaded region, representing allowed height-above-buoyancy–water depth combinations (without crevasses). The upper limit when crevasses are included (dashed line) passes through most of the data points, capturing the trend in the observations towards decreasing height-above-buoyancy with increasing water depth. This trend also compares remarkably well with a constant height-above-buoyancy of 50 m (dotted line) that has been suggested by some modellers, although this model assumes that calving occurs if the ice thickness is less than this critical thickness (Van der Veen 1996). The close connection between the two disparate theories is intriguing. Our theory, however, has the advantage that it has a physical basis and can permit the formation of floating ice tongues, which are prohibited by the height-above-buoyancy model.

4. Discussion

The use of observations with errors to validate approximate theories is fraught with danger, not the least of which is due to our neglect of lateral shear stress and the approximate treatment of the penetration depth of crevasses. More sophisticated analysis of the stresses is possible. For example, a full Stokes model could be used to include the effect of lateral and bending stresses near the terminus (Hanson & Hooke 2003). With this looming caveat in mind, of the three strength models, S3 provides the best fit to the observations and is broadly consistent with independent laboratory measurements of the strength of ice, provided a thin water film lubricates any pre-existing or developing fault surface. Moreover, the trend towards decreasing height-above-buoyancy

evident in the observations emerges naturally in our theory as a consequence of the need for increased water pressure to balance the increased weight of the ice of thick glacier termini. In our theory, it is no coincidence that thick outlet glaciers (e.g. Jakobshavn Isbræ and the Helheim Glacier) are very close to flotation.

Irrespective of the choice of strength model, several basic features of the model remain qualitatively true: (i) an increase in ice thickness leads to decreased stability of the ice front, while an increase in water depth leads to increased stability at the calving front and (ii) once the ice thickness increases beyond a critical level, no stable terminus (floating or grounded) is possible. We predict that maximum terminus ice thickness should never exceed the critical ice thickness (approx. 900–1100 m for S3, depending on the amount of crevassing). A direct consequence of this prediction is that, when the ice thickness at the grounding line of ice tongues (or ice shelves that experience little buttressing) exceeds approximately 1000 m, the ice may fail catastrophically. In the light of recent measurements of the grounding line retreat of the Pine Island and Thwaites Glacier tongues (Rignot *et al.* 2002; Joughin *et al.* 2010), sustained retreat of both of these glaciers may expose a deep grounding line and we speculate that this has the potential to trigger a sustained calving-induced retreat similar to that currently occurring in Jakobshavn Isbræ.

(*a*) *Floating or grounded termini?*

The view that emerges from our upper bound is that, provided the ice thickness is less than the critical threshold to support a buoyant ice tongue, the increased stability associated with deeper water implies that tidewater glaciers should always form floating ice tongues. This stands in stark contrast to the pronounced lack of ice tongues in Greenland, Svalbard and Alaska.

To explain why many tidewater glaciers do not have floating termini, we are forced to invoke the possibility that crevasses in many tidewater glaciers penetrate deeper than predicted by the Nye crevasse depth theory. We speculate that, in temperate glaciers, ample surface melt may enable surface crevasses to penetrate much deeper into the ice and that extensive englacial fracturing may further weaken the ice beyond what we predict using the dry crevasse penetration depths. Because extensive englacial fractures have been observed in temperate glaciers (Fountain & Walder 1998), this appears to be plausible for warm environments. Elsewhere, stresses upstream of the calving front may be sufficient to cause the ice entering the terminus to be crevassed more deeply than would be expected solely from consideration of the stresses near the terminus. This view also has support from field observations where crevasses are found to persist when they advect into compressive regions of flow (Mottram & Benn 2009). This hypothesis could be tested by examining crevasse penetration depths determined from ground-penetrating radar in the vicinity of glaciers that form floating ice tongues and those that do not. For instance, in S3, with an ice thickness of 1000 m, crevasses need to penetrate only slightly more than predicted by the Nye crevasse theory, (about 55%) for a floating ice tongue to be unstable. For a 400 m thick ice, front crevasses must penetrate more than 80 per cent of the ice thickness. Examining ground-penetrating radar observations of crevasse depths across ice tongues and tidewater glaciers may provide a significant test of the viability of

the theory, but it strongly indicates that ice tongues are most likely to form in regions where the ice is thin enough that shear stresses (and crevasse depths) are small.

(*b*) *A lower bound on the ice thickness at the termini of grounded tidewater glaciers*

The previous discussion suggests that floating ice tongues cannot form when the ice in the near-terminus region is deeply crevassed. This suggests that a heuristic lower bound on ice thickness at the terminus can be obtained by assuming that ice at the terminus is already entirely fractured to the point that the ice effectively has no cohesion ($C_0 = 0$). We again invoke Coulomb's law, this time omitting cohesion, but we now include friction and the effect of pore pressure in the submerged portion of the ice into Coulomb's law. Hence, the yield strength becomes

$$\tau_c = \mu[\rho g(H - z) - \rho_w g(D - z)], \quad z < D \tag{4.1}$$

and

$$\tau_c = \mu\rho g(H - z), \quad z \geq D, \tag{4.2}$$

where the symbol μ has been introduced to denote that the coefficient of friction of ice that has already failed may be different from the coefficient of friction of intact ice (Schulson 2001) and we have assumed that the pore pressure of water is equivalent to the hydrostatic pressure of the ocean directly adjacent to the glacier terminus. With the omission of cohesion and addition of pore pressure, the yield strength of ice now vanishes when the pore pressure of the water exactly balances the weight of the ice (i.e. when the ice becomes buoyant).

Our heuristic lower bound now proceeds by assuming a bottom-up failure mechanism whereby the entire ice cliff fails when the bottom of the ice reaches the yield stress. (This should be contrasted with the previous assumption that the ice cliff fails when the depth-averaged stress exceeds the depth-averaged yield stress.) The yield strength at the bottom of the ice is given by

$$\tau_c(z = 0) = \mu\rho_i g H \left[1 - \frac{\rho_w}{\rho_i}\frac{D}{H}\right], \tag{4.3}$$

and we require that this yield strength exceeds the shear stress within the ice such that

$$\frac{1}{2}\rho_i g H \left[1 - \frac{\rho_w}{\rho_i}\left(\frac{D}{H}\right)^2\right] \leq \mu\rho_i g H \left[1 - \frac{\rho_w}{\rho_i}\frac{D}{H}\right]. \tag{4.4}$$

Note that, because the yield strength at the bottom of the ice vanishes at buoyancy, a fully buoyant ice terminus will always be unstable and a floating ice tongue is prohibited in this limit.

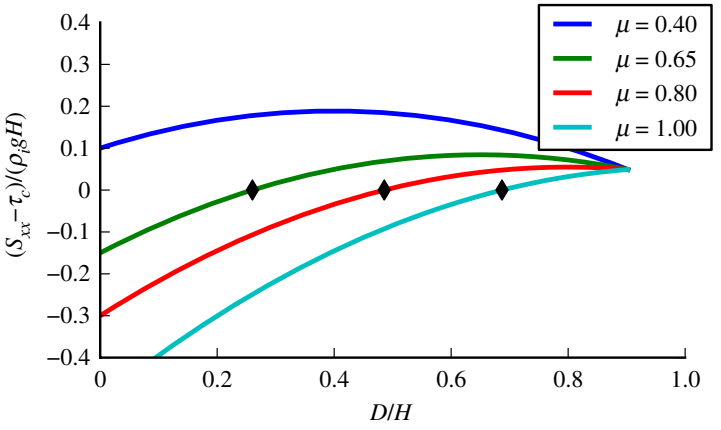

Figure 6. Failure of the ice cliff near the bed for a granular material as a function of different coefficients of friction. In the absence of cohesion, pore pressure will result in a yield strength that increases with increasing water depth, with zero strength of the ice occurring when the ice reaches buoyancy. Black diamonds show the maximum ratio of water depth to ice thickness possible for different coefficients of friction.

After some manipulation, the lower bound on ice thickness can be succinctly expressed as a constant fraction of water depth that depends on the coefficient of friction μ

$$\frac{D}{H} = \mu - \sqrt{\mu^2 + \frac{\rho_i}{\rho_w}(1-2\mu)}, \tag{4.5}$$

where we have kept only the geophysically relevant solution where the ratio of water depth to ice thickness is less than flotation. Figure 6 shows the difference between the shear stress and the yield stress at the bottom of the ice normalized by the hydrostatic weight of the ice for various coefficients of friction. For a coefficient of friction $\mu \leq 0.5$, no stable terminus in water is possible. This is analogous to the hydrophobic boundary condition used in some ice sheet models that forbid the advance of the ice front into water. In contrast, for $\mu \geq 1$ the terminus is stable until buoyancy is approached. Using a coefficient of friction of $\mu = 0.65$ (similar to S1) implies that the ice will fail when the ice terminates in water depth greater than about 25 per cent of the ice thickness. The lower bound appears to be unrealistically low for reasonable coefficients of friction. Although unsatisfying, this is consistent with it being a lower bound. Nonetheless, the lower bound provides ice sheet modellers with a convenient and easily implemented method of exploring limits on the magnitude of retreat possible using limiting assumptions about the coefficient of friction.

(*c*) *Rifting and the detachment of tabular bergs from ice shelves and ice tongues*

As previously emphasized, our theory predicts that grounded tidewater glaciers with sufficiently thick termini will fail either entirely by shear or by forming faults that connect pre-existing closely spaced surface crevasses with bottom crevasses. This will result in icebergs that have characteristic size of the order of or less

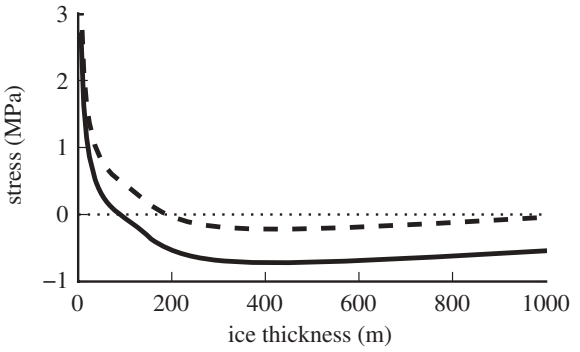

Figure 7. Shear stress minus cohesive stress calculated for S3, including the effect of ocean swell-induced flexural stresses. The flexural stresses were calculated using the maximum tensile stress induced from ocean swell wavelengths ranging from 100 to 750 m, each with an amplitude of 2 m. Young's modulus and Poisson's ratio were taken to be 10 GPa and 0.3, respectively (solid line, without crevasses; dashed line, with crevasses).

than the ice thickness. However, a direct consequence of the fact that floating ice tongues–shelves less than the critical thicknesses are intrinsically stable compared with their grounded brethren is that shear failure is much less likely. The stability of the calving front may explain the paucity of small icebergs shed from the calving front of floating ice tongues/shelves in comparison with discharge of icebergs from grounded glaciers.

Calving from ice shelves/tongues is instead dominated by the detachment of large tabular bergs from rift systems that can initiate far upstream of the calving front and then slowly advect downstream for decades. Our analysis does not treat the formation of these rifts explicitly (this would require a numerical ice shelf model to resolve internal stresses); once a rift initiates, the rift–wall–ocean boundary is analogous to the ice–ocean boundary at the calving front. Although our analysis is silent about the source of the stress concentration that causes rifts to initiate in the first place, we predict that, once a rift forms in an ice shelf, it is stable to rift wall collapse. It is this feature that may enable rifts to not only exist, but also propagate for decades. In contrast, rifts that initiate upstream of the calving front of tidewater glaciers are not necessarily stable and can only form in tidewater glaciers that are very thin or have termini very close to flotation.

(*d*) *The role of ocean swell in triggering calving events from ice tongues and ice shelves*

Several authors have suggested that calving from ice shelves and ice tongues may be triggered by flexural stresses induced by ocean swell (Holdsworth & Glynn 1978; MacAyeal *et al.* 2006; Sergienko 2010), despite some contradictory observations that ice shelf rift propagation itself is not influenced by ocean swell (Bassis *et al.* 2007, 2008). To examine the role of ocean swell in generating transient stresses that contribute to failure of floating ice tongues, we estimated the magnitude of the horizontal stress induced in the ice following the order of magnitude estimation procedure described by Bassis *et al.* (2007, 2008). The stress due to ocean swell is taken as the maximum stress imparted to the

ice, assuming wavelengths for ocean swell that range from 100 to 750 m (all within the most energetic portion of the ocean swell spectrum) and assuming an amplitude of 2 m (comparable to significant wave heights). Figure 7 shows the difference between the shear stress and the yield strength for S3 as a function of ice shelf thickness, including the effect of flexure. The effect of ocean swell is modest for thick ice shelves where the flexural wavelength of ice is large compared with that of the incident swell. However, for thin ice shelves–tongues with ice thickness less than about 200 m, ocean swell has a wavelength that is comparable to the flexural wavelength of ice and is sufficient to cause failure of thin ice shelves. This crude calculation provides a possible link to the anecdotal reports of ice shelf calving during periods when the sea ice buttressing the shelf from incoming pulses of ocean swell blows out. This also suggests that ocean swell is of greatest importance for thin ice shelves. More elaborate models that explicitly account for seafloor topography, ice shelf morphology and the energy spectrum are possible (Sergienko 2010), but are beyond the scope of the current study.

5. Conclusions

The upper bound for ice thickness developed in this study matches observed ice thickness–water depth combinations remarkably well for a cohesive strength of 1 MPa and a relatively small coefficient of friction. This yield strength is consistent with laboratory measurements of the yield strength of ice, provided a thin lubricating water layer forms along the fracture or that failure is primarily plastic. A crucial difference between our approach and previous approaches is that we allow the ice to fail in both shear and tension. This negates the need to invoke surface meltwater to enable calving nor do we need to assume that surface crevasses and bottom crevasses somehow vertically intersect.

In contrast to previous models, our upper bound predicts a maximum ice cliff height for a stable calving cliff and this maximum height increases with increasing water depth, leading towards a trend of decreasing height-above-buoyancy that is closely matched by observations. In our theory, the decrease in height-above-buoyancy is a consequence rather than a cause of the retreat. Our analysis also predicts that, as long as the ice is sufficiently intact and thin enough to support a floating ice tongue, a floating terminus is the most stable configuration. The existence of a floating ice tongue, however, is contingent on relatively intact ice and crevasses that are either widely spaced and/or do not penetrate substantially deeper than predicted by the Nye crevasse depth model. We speculate that the increased stability associated with a floating calving front may explain why floating ice tongues calve comparatively few ice thickness-sized bergs in comparison with tidewater glaciers of similar thickness. However, we have also shown that thin ice tongues are also more sensitive to ocean swell-induced flexural stresses and that these may contribute to failure when the ice tongue is exposed to wave action.

To explain the observation that some glaciers calve most vigorously when they approach buoyancy, we were forced to assume that the ice was already heavily fractured and, by approximating the ice as a granular material, we were able to obtain a lower bound on the terminus stability. The lower bound

yields a prediction in which increasing water depth decreases the strength of the ice, leading to decreased stability and calving behaviour similar to previously proposed height-above-buoyancy calving laws. Combining the upper and lower bound provides boundary conditions and limits that can be used by ice sheet modellers to probe upper and lower limits of plausible retreat scenarios in regional and/or continental-scale ice sheets models. This may provide a physical basis to explore upper and lower limits of plausible glacier retreat scenarios in numerical ice sheet models to probe the probable limits of ice sheet response to warming in the coming centuries.

We are sincerely grateful for the careful reviews of the editor and two anonymous reviewers, whose comments significantly improved the clarity of this manuscript. This work was supported by NASA through grant NNX08AN59G and NSF grant ARC1064535.

References

Bassis, J. 2010 Hamilton-type principles applied to ice-sheet dynamics: new approximations for large-scale ice-sheet flow. *J. Glaciol.* **56**, 497–513. (doi:10.3189/002214310792447761)

Bassis, J. 2011 The statistical physics of iceberg calving and the emergence of universal calving laws. *J. Glaciol.* **57**, 3. (doi:10.3189/002214311795306745)

Bassis, J. N., Coleman, R., Fricker, H. A. & Minster, J. B. 2005 Episodic propagation of a rift on the Amery Ice Shelf, East Antarctica. *Geophys. Res. Lett.* **32**, L02502. (doi:10.1029/2004GL022048)

Bassis, J., Fricker, H., Coleman, R., Bock, Y., Behrens, J., Darnell, D., Okal, M. & Minster, J. 2007 Seismicity and deformation associated with ice-shelf rift propagation. *J. Glaciol.* **53**, 523–536. (doi:10.3189/002214307784409207)

Bassis, J., Fricker, H., Coleman, R. & Minster, J. 2008 An investigation into the forces that drive ice-shelf rift propagation on the Amery Ice Shelf, East Antarctica. *J. Glaciol.* **54**, 17–27. (doi:10.3189/002214308784409116)

Beeman, M., Durham, W. & Kirby, S. 1988 Friction of ice. *J. Geophys. Res.* **93**, 7625–7633. (doi:10.1029/JB093iB07p07625)

Benn, D., Warren, C. & Mottram, R. 2007 Calving processes and the dynamics of calving glaciers. *Earth Sci. Rev.* **82**, 143–179. (doi:10.1016/j.earscirev.2007.02.002)

Brown, C. S., Meier, M. F. & Post, A. 1982 Calving speed of Alaska tidewater glaciers, with applications to Columbia Glacier. *U.S. Geol. Surv. Prof. Paper* **1258C**, 13.

Dowdeswell, J. & Drewry, D. 1989 The dynamics of Austfonna, Nordaustlandet, Svalbard: surface velocities, mass balance, and subglacial melt water. *Ann. Glaciol.* **12**, 37–45.

Fountain, A. G. & Walder, J. S. 1998 Water flow through temperate glaciers. *Rev. Geophys.* **36**, 299–328. (doi:10.1029/97RG03579)

Gagno, R. & Gi, P. 1995 Characterization and flexural strength of iceberg and glacier ice. *J. Glaciol.* **41**, 995.

Hanson, B. & Hooke, R. 2003 Buckling rate and overhang development at a calving face. *J. Glaciol.* **49**, 577–586. (doi:10.3189/172756503781830476)

Holdsworth, G. & Glynn, J. 1978 Iceberg calving from floating glaciers by a vibrating mechanism. *Nature* **274**, 464–466. (doi:10.1038/274464a0)

Howat, I. M., Joughin, I., Tulaczyk, S. & Gogineni, S. 2005 Rapid retreat and acceleration of Helheim Glacier, east Greenland. *Geophys. Res. Lett.* **32**, 22502. (doi:10.1029/2005GL024737)

Hughes, T. & Nakagawa, M. 1989 Bending shear: the rate-controlling mechanism for calving ice walls. *J. Glaciol.* **35**, 260–266.

Jezek, K. 1984 A modified theory of bottom crevasses used as a means for measuring the buttressing effect of ice shelves on inland ice sheets. *J. Geophys. Res.* **89**, 1925–1931. (doi:10.1029/JB089iB03p01925)

Joughin, I. & MacAyeal, D. R. 2005 Calving of large tabular icebergs from ice shelf rift systems. *Geophys. Res. Lett.* **32**, 2501. (doi:10.1029/2004GL020978)

Joughin, I., MacAyeal, D. R. & Tulaczyk, S. 2004 Basal shear stress of the Ross ice streams from control method inversions. *J. Geophys. Res.* (*Solid Earth*) **109**, 9405. (doi:10.1029/2003JB002960)

Joughin, I., Das, S., King, M., Smith, B., Howat, I. & Moon, T. 2008 Seasonal speedup along the western flank of the Greenland ice sheet. *Science* **320**, 781–783. (doi:10.1126/science.1153288)

Joughin, I., Smith, B. & Holland, D. 2010 Sensitivity of 21st century sea level to ocean-induced thinning of Pine Island Glacier, Antarctica. *Geophys. Res. Lett.* **37**, 20. (doi:10.1029/2010GL044819)

Kennedy, F., Schulson, E. & Jones, D. 2000 The friction of ice on ice at low sliding velocities. *Philos. Mag. A* **80**, 1093–1110. (doi:10.1080/01418610008212103)

Krimmel, R. 2001 Photogrammetric data set, 1957–2000, and bathymetric measurements for Columbia Glacier, Alaska. Inv. Report no. 01-4089. USGS Water Resource, Reston, VA.

Lazzara, M., Jezek, K., Scambos, T., MacAyeal, D. & Van der Veen, C. 1999 On the recent calving of icebergs from the Ross Ice Shelf. *Polar Geogr.* **23**, 201–212. (doi:10.1080/10889379909377676)

Lefauconnier, B., Hagen, J. & Rudant, J. 1994 Flow speed and calving rate of Kongsbreen Glacier, Svalbard, using spot images. *Polar Res.* **13**, 59–65. (doi:10.1111/j.1751-8369.1994.tb00437.x)

Luckman, A. & Murray, T. 2005 Seasonal variation in velocity before retreat of Jakobshavn Isbræ, Greenland. *Geophys. Res. Lett.* **32**, L08501. (doi:10.1029/2005GL022519)

MacAyeal, D. 1989 Large-scale ice flow over a viscous basal sediment: theory and application to ice stream B, Antarctica. *J. Geophys. Res.* **94**, 4071–4087. (doi:10.1029/JB094iB04p04071)

MacAyeal, D. *et al.* 2006 Transoceanic wave propagation links iceberg calving margins of Antarctica with storms in tropics and Northern Hemisphere. *Geophys. Res. Lett.* **33**, L17502. (doi:10.1029/2006GL027235)

Meier, M. F. & Post, A. 1987 Fast tidewater glaciers. *J. Geophys. Res.* **92**, 9051–9058. (doi:10.1029/JB092iB09p09051)

Mottram, R. & Benn, D. 2009 Testing crevasse-depth models: a field study at Breiethamerkurjokull, Iceland. *J. Glaciol.* **55**, 746–752. (doi:10.3189/002214309789470905)

Nick, F., Vieli, A., Howat, I. & Joughin, I. 2009 Large-scale changes in Greenland outlet glacier dynamics triggered at the terminus. *Nat. Geosci.* **2**, 110–114. (doi:10.1038/ngeo394)

Nick, F., van der Veen, C., Vieli, A. & Benn, D. 2010 A physically based calving model applied to marine outlet glaciers and implications for the glacier dynamics. *J. Glaciol.* **56**, 781–794. (doi:10.3189/002214310794457344)

Nye, J. F. 1957 The distribution of stress and velocity in glaciers and ice-sheets. *Proc. R. Soc. Lond. A* **239**, 113–133. (doi:10.1098/rspa.1957.0026)

Nye, J. *et al.* 1952 The mechanics of glacier flow. *J. Glaciol.* **2**, 82–93.

Pelto, M. S. & Warren, C. R. 1991 Relationship between tidewater glacier calving velocity and water depth at the calving front. *Ann. Glaciol.* **15**, 115–118.

Press, W., Teukolsky, S., Vetterling, W. & Flannery, B. 1992 *Numerical recipes in C*. Cambridge UK: Cambridge University Press.

Reeh, N. 1968 On the calving of ice from floating glaciers and ice shelves. *J. Glaciol.* **7**, 215–232.

Rignot, E., Vaughan, D. G., Schmeltz, M., Dupont, T. & MacAyeal, D. 2002 Acceleration of Pine Island and Thwaites Glaciers, West Antarctica. *Ann. Glaciol.* **34**, 189–194. (doi:10.3189/172756402781817950)

Rignot, E., Casassa, G., Gogineni, P., Krabill, W., Rivera, A. & Thomas, R. 2004 Accelerated ice discharge from the Antarctic Peninsula following the collapse of Larsen B ice shelf. *Geophys. Res. Lett.* **31**, 18401. (doi:10.1029/2004GL020697)

Rist, M., Sammonds, P., Oerter, H. & Doake, C. 2002 Fracture of Antarctic shelf ice. *J. Geophys. Res.* **107**, 13. (doi:10.1029/2000JB000058)

Scambos, T., Hulbe, C. & Fahnestock, M. 2003 Climate-induced ice shelf disintegration in the Antarctic peninsula. *Antarct. Res. Ser.* **79**, 79–92. (doi:10.1029/AR079p0079)

Scambos, T. A., Bohlander, J. A., Shuman, C. A. & Skvarca, P. 2004 Glacier acceleration and thinning after ice shelf collapse in the Larsen B embayment, Antarctica. *Geophys. Res. Lett.* **31**, L18402. (doi:10.1029/2004GL020670)

Schulson, E. M. 2001 Brittle failure of ice. *Eng. Fract. Mech.* **68**, 1839–1887. (doi:10.1016/S0013-7944(01)00037-6)

Schulson, E. & Duval, P. 2009 *Creep and fracture of ice*. Cambridge, UK: Cambridge University Press.

Sergienko, O. 2010 Elastic response of floating glacier ice to impact of long-period ocean waves. *J. Geophys. Res.* **115**, F04028. (doi:10.1029/2010JF001721)

Skvarca, P., de Angelis, H., Naruse, R., Warren, C. R. & Aniya, M. 2002 Calving rates in fresh water: new data from southern Patagonia. *Ann. Glaciol.* **34**, 379–384. (doi:10.3189/172756402781817806)

Turcotte, D. L. & Schubert, G. 2002 *Geodynamics*. Cambridge, UK: Cambridge University Press.

Van der Veen, C. J. 1996 Tidewater calving. *J. Glaciol.* **42**, 375–385.

Van der Veen, C. J. 2002 Calving glaciers. *Prog. Phys. Geogr.* **26**, 96–122. (doi:10.1191/0309133302pp327ra)

Vaughan, D. G. 1993 Relating the occurrence of crevasses to surface strain rates. *J. Glaciol.* **39**, 255.

Walter, F., O'Neel, S., McNamara, D., Pfeffer, W., Bassis, J. & Fricker, H. 2010 Iceberg calving during transition from grounded to floating ice: Columbia Glacier, Alaska. *Geophys. Res. Lett.* **37**, L15501. (doi:10.1029/2010GL043201)

Watts, A. 2001 *Isostasy and flexure of the lithosphere*. Cambridge, UK: Cambridge University Press.

Weertman, J. 1980 Bottom crevasses. *J. Glaciol.* **25**, 185–188.

Weiss, J. & Schulson, E. 2009 Coulombic faulting from the grain scale to the geophysical scale: lessons from ice. *J. Phys. D Appl. Phys.* **42**, 214017. (doi:10.1088/0022-3727/42/21/214017)